Proof-of-concept demonstration of edge-illumination x-ray phase contrast imaging combined with tomosynthesis



2014 Phys. Med. Biol. 59 N1

(http://iopscience.iop.org/0031-9155/59/5/N1)

OPEN ACCESS
IOP Publishing | Institute of Physics and Engineering in Medicine
Made open access 12 March 2014
Physics in Medicine and Biology
Phys. Med. Biol. **59** (2014) N1–N10
doi:10.1088/0031-9155/59/5/N1

**Note**

# Proof-of-concept demonstration of edge-illumination x-ray phase contrast imaging combined with tomosynthesis

**Magdalena B Szafraniec, Thomas P Millard, Konstantin Ignatyev[1], Robert D Speller and Alessandro Olivo[2]**

Department of Medical Physics and Bioengineering, UCL, London WC1E 6BT, UK

E-mail: a.olivo@ucl.ac.uk

Received 5 June 2013, revised 5 November 2013
Accepted for publication 8 November 2013
Published 20 February 2014

**Abstract**

In this note we present the first proof-of-concept results on the potential effectiveness of the edge-illumination x-ray phase contrast method (in its 'coded-aperture' based lab implementation) combined with tomosynthesis. We believe that, albeit admittedly preliminary (e.g. we only present phantom work), these results deserve early publication in a note primarily for four reasons. First, we fully modelled the imaging acquisition method, and validated the simulation directly with experimental results. This shows that the implementation of the method in the new geometry is understood, and thus that it will be possible to use the model to simulate more complex scenarios in the future. Secondly, we show that a strong phase contrast signal is preserved in the reconstructed tomosynthesis slices: this was a concern, as the high spatial frequency nature of the signal makes it sensitive to any filtration-related procedure. Third, we show that, despite the non-optimized nature of the imaging prototype used, we can perform a full angular scan at acceptable dose levels and with exposure times not excessively distant from what is required by clinical practice. Finally, we discuss how the proposed phase contrast method, unlike other approaches apart from free-space propagation (which however requires a smaller focal spot, thus reducing the flux and increasing exposure times), can be easily implemented in a tomosynthesis geometry suitable for clinical use. In summary, we find that these technical results indicate a high potential for the combination of the two methods. Combining slice separation with detail enhancement provided by phase effects would substantially increase the detectability of small lesions

[1] Present address: Diamond Light Source, Harwell Science and Innovation Campus, Didcot, OX11 0DE, UK.
[2] Author to whom any correspondence should be addressed.

0031-9155/14/050001+10$33.00  

and/or calcifications, which we aim to demonstrate in the next steps of this study.

(Some figures may appear in colour only in the online journal)

## Introduction

This note presents preliminary results on the possible combination of two important developments in medical x-ray imaging, namely x-ray phase contrast imaging (XPCi) (Lewis 2004, Bravin *et al* 2013) and digital tomosynthesis (DTS) (Dobbins and Godfrey 2003, Park *et al* 2007).

Following its introduction either at synchrotrons (Snigirev *et al* 1995, Ingal and Beliaevskaya 1995) or with microfocal sources (Davis *et al* 1995, Wilkins *et al* 1996), XPCi has progressed significantly over recent years. Most importantly, methods have emerged that enable its implementation with conventional, non-microfocal laboratory sources, such as Talbot–Lau interferometry (Pfeiffer *et al* 2006) and edge-illumination/coded-aperture approaches (Olivo *et al* 2001, Olivo and Speller 2007a). These methods have the potential to enable the transfer of XPCi into clinical practice.

This note focuses on the latter method, primarily because of its simplified set-up (Olivo *et al* 2011a), which however does not affect its phase sensitivity (Marenzana *et al* 2012). Specifically with regards to a tomosynthesis implementation, this set-up simplification is essential as it enables acquiring the various projections simply by 'tracking' the source angular position with a lateral displacement of the pre-sample mask (see below).

The method is based on the 'edge-illumination' principle, i.e. the observation that illuminating only the edge of the detector pixels substantially enhances the phase sensitivity of an x-ray imaging system. It was first introduced in the framework of a synchrotron experiment (Olivo *et al* 2001), and more recently adapted for use with conventional sources by means of a pair of appropriately designed apertured masks placed either side of the imaged object (Olivo and Speller 2007a; a schematic of the imaging system is presented in the next section). A recent paper reviews the two implementations of the method, and discusses the transition from one to the other (Munro *et al* 2012b).

The lab-based set up was shown to provide intense XPCi signals also when used with focal spots of up to 100 $\mu$m, compatible with current practice in mammography (Olivo and Speller 2007b), to easily tolerate high x-ray energies (Ignatyev *et al* 2011a) and to be resilient to misalignments/vibrations of the order of a few $\mu$m (Olivo *et al* 2011a). Again this is an essential feature in view of a tomosynthesis implementation, as this sort of tolerance is within reach of current technology; for comparison, Talbot–Lau methods were shown to require tolerances of a few tens of nm (Zambelli *et al* 2010). Finally, the low aspect ratio of the masks makes them cheap and easy to fabricate, and mask areas sufficient to cover large fields of view are already commercially available.

Edge-illumination XPCi produces differential phase contrast profiles through integration (at the pixel level) of partial free-space propagation profiles, in themselves proportional to the second derivative of the phase shift (Olivo and Speller 2008, Munro *et al* 2012b). The final result practically matches the signal that is obtained in analyser based imaging (Davis *et al* 1995, Ingal and Beliaevskaya 1995, Chapman *et al* 1997): this was already recognized in the original edge-illumination paper (Olivo *et al* 2001), and was more recently formally demonstrated (Munro *et al* 2013). Due to this corpus of previous literature, and in the interest of brevity as required by a note, formal equations expressing the x-ray intensity detected at

the pixel level will not be repeated here—explicit expressions can be found in Munro *et al* 2010, 2012a, Diemoz *et al* 2013. Phase retrieval (Munro *et al* 2012a) was not performed in the present case, hence the images presented below contain the differential phase signal superimposed on the 'standard' absorption one. This is essentially the strategy followed by the *in vivo* program underway at the Trieste synchrotron (Castelli *et al* 2011), and was adopted primarily for its simplicity and because it enabled us to keep dose and exposure time to a minimum. At the same time, it is admittedly a limiting approach, as it prevents the application of promising algorithms like, for example, the one recently introduced by Köhler *et al* (2011), as they require the prior separation of phase and absorption signals. Phase retrieval methods are a relatively recent development for our method (Munro *et al* 2012a, 2013), and more research in this direction will be undertaken in the next stages of this preliminary study.

DTS provides separated volumetric image slices of the sample in planes perpendicular to the 'main' x-ray direction (bisector of the angle spanned by the source during the scan) through limited view tomography. This enables removing, or at least suppressing, the 'structural noise' due to the superposition of multiple anatomic structures projected onto the same region of the image, which could mask the details of interest (Dobbins and Godfrey 2003, Park *et al* 2007). While DTS finds several applications in diagnostic radiology, breast imaging is considered one of the most significant as DTS can at least partially solve the well-known 'dense breast' problem, in which the superposition of fibroglandular structures can make it difficult to visualize faint tumours in individual 2D projection images (Niklason *et al* 1997).

While several acquisition geometries exist for DTS, such as fully (Dobbins and Godfrey 2003) and partially isocentric (Dobbins and Godfrey 2003, Niklason *et al* 1997), in this preliminary study conducted with a proof-of-concept prototype we have decided to rotate the sample over a limited angular range, while keeping source, aperture masks and detector stationary. This effectively corresponds to the fully isocentric geometry, and the adaptation to more sophisticated geometries (as well as direct testing of the case in which the sample is kept stationary and the tube rotated) will be the subject of future research.

## Materials and methods

Figure 1 shows a schematic of the imaging prototype. This uses the Rigaku M007 rotating target x-ray source, with a molybdenum anode and a focal spot size of approximately 75 $\mu$m. For this experiment, it was operated at 40 kVp and 25 mA with 30 $\mu$m Mo filtration. The detector is the ANRAD 'SMAM' amorphous selenium flat panel, with a pixel size of 85 $\mu$m.

Both detector and pre-sample aperture masks were manufactured to the authors' design by Creatv Microtech (Potomac, MD, USA). The detector mask consists of a series of 720 $\times$ 6 cm long vertical 20 $\mu$m wide apertures, with 83.5 $\mu$m pitch, obtained in an approximately 30 $\mu$m thick gold layer electroplated on a graphite substrate. The pre-sample mask has the same design demagnified by a factor 1.25 to account for the beam divergence—source-to-sample and sample-to-detector distances were 1.6 and 0.4 m respectively in this case. Both masks are mounted on a stack of Newport translators and Kohzu cradles which allows the alignment of each aperture with a pixel column in the detector (Ignatyev *et al* 2013). Images were obtained at '50% illumination' (Olivo and Speller 2007b), which means that the two masks were misaligned by half an aperture size along $x$ (see figure 1(b)). The sample stage features translation along $x$, rotation around $y$ for the tomosynthesis acquisitions, and cradles allowing rotation along $z$ and $x$ to enable alignment of the tomosynthesis rotation axis ($y$) with the pixel columns.

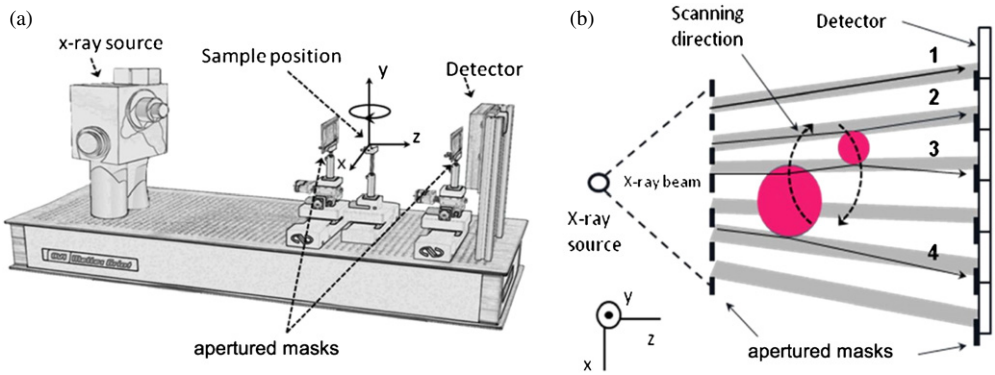


**Figure 1.** The imaging prototype. (a) Pictorial representation with (from left to right) source, pre-sample mask, sample stage, detector mask and detector, mounted on an optical table. (b) Schematic representation (not to scale) showing how the pre-sample mask splits the beam into individual beamlets, how each one of these hits the transition between a sensitive and an insensitive area on the detector as defined by the detector mask (thus realizing the 'edge-illumination' condition), and how each one of these can be deviated by the sample thus creating positive or negative phase fringes.

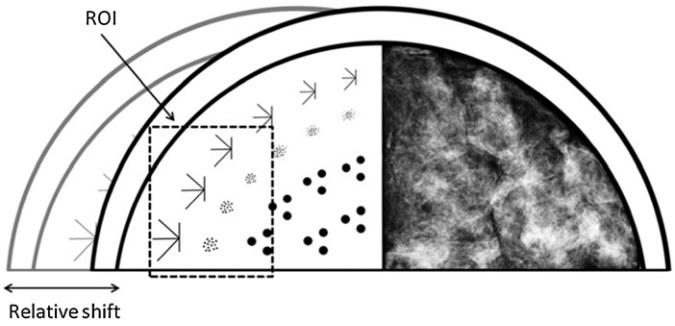


**Figure 2.** The 'double TORMAM' phantom, featuring a total thickness of 3.2 cm. The dashed box highlights the ROI imaged in this experiment.

Two phantoms were imaged—one aimed at experimentally verifying the developed simulations and the other at testing the imaging system on a sample of sufficient thickness. The 'simulation' phantom ('wire phantom' in the following) consisted of two polyethylene wires (roughly) aligned in the $y$ direction, separated by 2 cm, with thicknesses of 210 and 470 $\mu$m respectively. This was mounted on the sample stage with the centre of rotation (approximately) between the two wires. The second phantom ('double TORMAM' in the following) was obtained by superimposing two TORMAM mammography phantoms (Leeds Test Objects Ltd, Boroughbridge, Yorkshire, UK) and shifting them one with respect to the other, so that different details overlapped in an individual projection image. Each phantom is 1.6 cm thick, for an overall sample thickness of 3.2 cm. Figure 2 shows the sample and the region of interest (ROI) imaged in this experiment.

Two different strategies were followed (and ultimately compared) to simulate the wire phantom. The first one was based on an extension of the ray optics model described in Olivo and Speller (2007b). This extension allows following each ray after interaction with the first object, calculating possible interactions with the second object and tracking the (twice) modified trajectory to verify whether it hits a detector aperture or the solid septa between

apertures (e.g. see trajectory '3' in figure 1(b)). By changing the position of the centres of the two wires (which are given as input to the code), the double wire combination can be rotated, thus simulating the various projections forming the tomosynthesis scan. The second strategy consisted in implementing the appropriate geometry through the modular Monte Carlo 'McXtrace' program (Knudsen *et al* 2011). Considering that the Olivo and Speller model had been experimentally verified a number of times in the past (Olivo and Speller 2007b, Ignatyev *et al* 2011a, 2011b, Olivo *et al* 2011b), this also enabled us to 'benchmark' the McXtrace software, which means that in the future we will be able to reliably exploit its modular nature and flexibility to simulate more complex scenarios.

The measurement of the entrance dose was obtained with a calibrated ionization chamber (Keithley 35050A) placed behind the pre-sample mask and in contact with the phantom. A value of 0.76 mGy was measured at zero degree projection angle for a 7 s exposure (see figures 5 and 6 below and related discussion), and multiplied by the number of angles to obtain a total air kerma used in the tomosynthesis scan. As the key results presented below for the 3.2 cm thick 'double TORMAM' phantom were obtained using 15 projections, this corresponds to a total entrance dose of 11.4 mGy for the entire DTS scan, which is within the limits of quality assurance protocols in mammography (Gennaro *et al* 2004).

Images were reconstructed using an iterative algorithm based on the separable paraboidal surrogates method developed by Sotthivirat and Fessler, a full description of which can be found in Erdogan and Fessler (1999), Fessler and Erdogan (1999) and Sotthivirat and Fessler (2000). The convergence check was performed visually: we observed that ten iterations were typically sufficient to enhance the phase contrast signal without compromising image quality through excessively increased noise. The resolution in the $z$ direction was set to 0.5 mm. Prior to reconstruction, all projections were dark- and bright-field corrected, i.e. the 'dark' image acquired with the beam off was subtracted, and the result was then normalized to the 'bright' field image acquired with the beam on but without the sample present. The reconstruction method was chosen because its use resulted in better image quality and preservation of the phase-induced edge-enhancement compared to the other methods we tested (e.g. filtered backprojections).

As done above for the expressions of x-ray intensity at the pixel level, due to the brevity constraints imposed by a note we avoid repeating the reconstruction equations here, and refer the reader to the quoted literature. It should be noted that the development of a dedicated reconstruction algorithm was not among the aims of the present proof-of-concept work, although this might be pursued as a future direction (e.g. along the lines described by Köhler *et al* (2011), following incorporation of phase retrieval in an efficient tomosynthesis acquisition scheme). Our aim thus far was to implement the edge-illumination XPCi method in the tomosynthesis geometry while choosing the reconstruction algorithm providing the best performance for 'mixed' phase/absorption images (Castelli *et al* 2011) among the ones available.

## Results and discussion

Figure 3 shows the comparison between experimental and simulated (with both the Olivo and Speller ray tracing and McXtrace models) profiles extracted from projection images of the wire phantom, rotated at different angles.

As can be seen, the two simulation models provide practically indistinguishable results, which enables us to benchmark McXtrace against an existing model that was previously experimentally verified. Most importantly, there is good match with the experimental results. In the interest of brevity, only two examples are reported, but the full tomosynthesis scan was simulated, and the same agreement was observed at all angles.

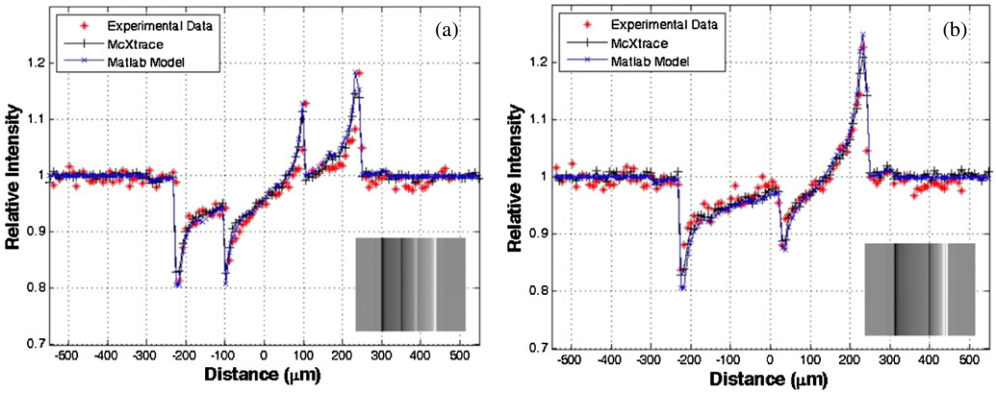


**Figure 3.** Two examples of the matching between the two simulation models (Olivo and Speller, blue line with small crosses, and McXtrace, black line with vertical bars) and the experiment (red stars). In (a), the rotation angle is such that the small wire is projected roughly at the centre of the large one. In (b), the right edges almost match, and as a consequence the positive peak on the right-hand side of the profile is amplified. The small insets show the (simulated) images for each case.

Figure 4 shows the slices reconstructed from simulated (panels (a) and (d) and experimental (panels (b) and (e)) tomosynthesis scans of the wire phantom. The scan was limited to angular positions where wires overlap, i.e. broadly speaking from the position represented in figure 3(b) to the symmetric one where the left edges of the wires overlap. This required an angular span of approximately 1.5°, which was covered through 15 angular steps of approximately 0.1° each.

Despite the limited angular range and the fact that the two wires are always completely overlapping in the individual projections, they are fully separated in the tomosynthesis reconstruction. Most importantly, the phase-induced edge-enhancement is preserved, and despite the additional steps of acquiring multiple projections and performing a tomosynthesis reconstruction, there is still optimal agreement between simulated and experimental data extracted from reconstructed slices (profiles in figures 4(c) and (f)), although the noise is increased and some reconstruction artefacts can be observed. This further validates the robustness and reliability of the simulation model(s).

Due to the small dimensions of the imaged details, and for the sake of a better comparison between simulation and experiment, the sample was 'dithered' in four steps for each angular projection, i.e. the sample was laterally displaced by a quarter of a (demagnified) pixel, and an image with increased resolution was obtained for each projection by recombining the four sub-pixel images. This means that 4 (dithering steps) $\times$ 15 (angular projection) $=$ 60 images were acquired in total, for an overall scan time of 3′ (the exposure time for each frame being 3 s). This 'dithering' process was not applied to the 'double TORMAM' images presented below, which enabled us to reduce both exposure time and delivered dose.

The 'double TORMAM' phantom was acquired in 15 projections of 1° each, with a 7 s exposure per projection and no dithering, i.e. a single projection was acquired at each angular position. This corresponds to a total scan time of 105 s and a total entrance dose of 11.4 mGy (see above), compatible with quality assurance protocols in mammography (Gennaro *et al* 2004). The exposure time per frame was increased with respect to the wire phantom to compensate for the higher absorption of the 3.2 cm thick 'double TORMAM' phantom. However, it should be noted that this has not been optimized, and strategies exist to reduce the exposure time (e.g. we have evidence that the system length could be reduced

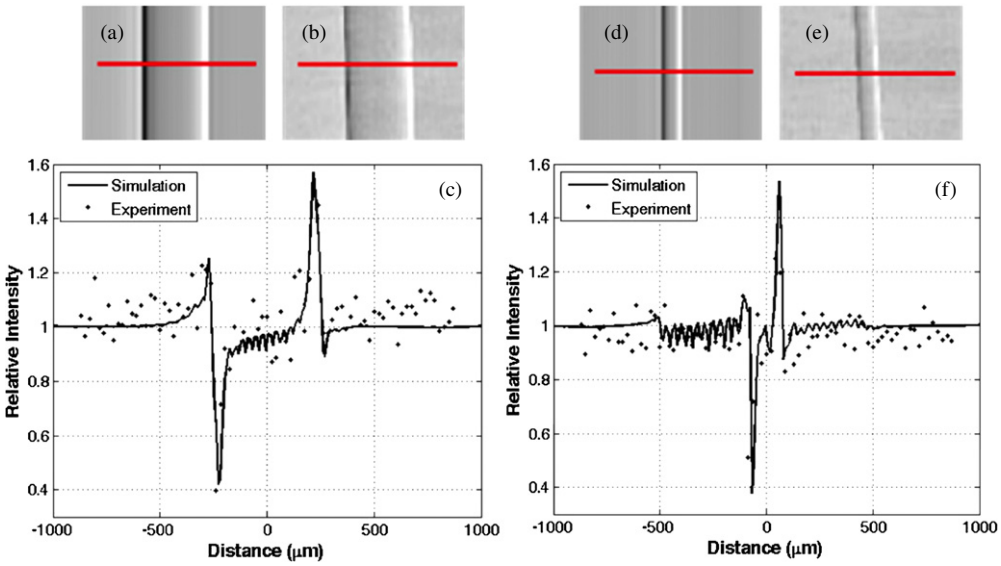


**Figure 4.** Reconstructed tomosynthesis slices of the wire phantom. (a) and (b) show the image slices, reconstructed from simulated and experimental data respectively, corresponding to the $z$ position of the thick wire; the horizontal line indicates the position where the profiles reported in (c) were extracted. Panels (d), (e) and (f) show the simulated image, experimental image and profiles (respectively) for the slice containing the thin wire. In both (c) and (f), solid lines and dots represent profiles extracted from simulated and experimental images respectively.

from the current 2 m to at least 1.5 m (Olivo and Speller 2007b)). A significant detail showing effective separation of features while preserving strong phase-related edge enhancement is shown in figure 5; for completeness' sake, figure 6 shows the full area of the phantom that has been imaged.

Admittedly, the imaged phantom represents a highly simplified imaging task compared to real breast tissue. However, we find that this study reaches its preliminary aim which was to demonstrate that our XPCi method can be implemented in tomosynthesis geometry while maintaining substantial phase-induced edge-enhancement and delivering radiation doses compatible with clinical requirements. While the phantom's simple geometrical structure is likely to have played a role in enabling a limited angular span, it should be noted that wider spans (and larger frame numbers) could be coupled to a lower exposure per frame to reach the same overall dosage, and therefore potentially similar statistics in the reconstructed slices. This will be the subject of further investigations.

Finally, we point out the simple way in which edge-illumination could be implemented in a tomosynthesis system in which the object is kept stationary and the source moves in an arc above it. The edge-illumination method requires only that the illuminated pixel fraction (i.e. the portion of each beamlet in figure 1(b) falling outside the absorbing septa of the detector mask) is kept constant at all projections. As the source position is moved along an arc, this is obtained by a lateral displacement of the pre-sample aperture. This displacement can be easily calculated in advance, and needs to be realized with a tolerance of 1–2 $\mu$m, which is within reach of current technology (Olivo *et al* 2011a). Most importantly, the detector output (e.g. outside the sample) is in itself a measure of the pre-sample mask position: this can be used in a feedback mechanism that tracks the pre-sample mask position and keeps the system dynamically aligned, as discussed in Ignatyev *et al* (2013).

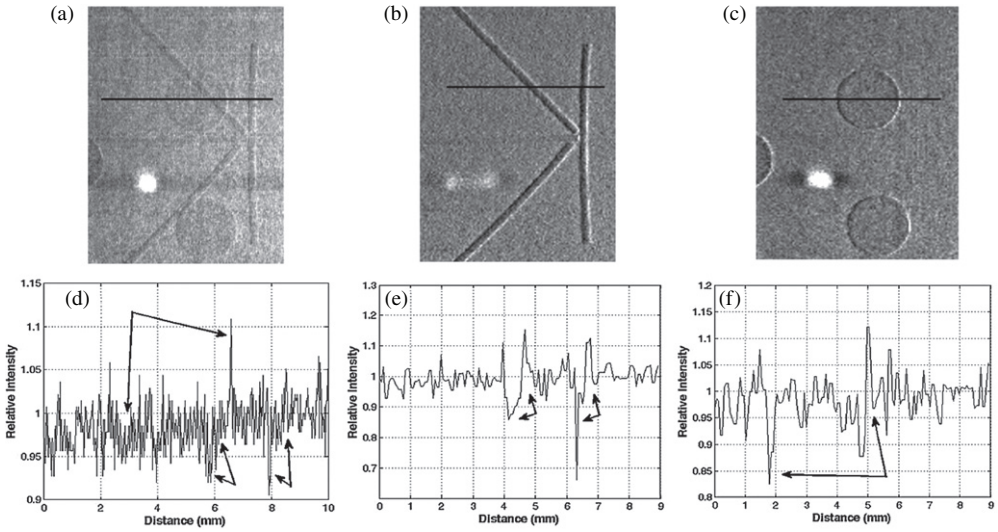


**Figure 5.** Detail of the 'double TORMAM' phantom, corresponding to an area where fibre and disc details overlap. (a) is the single projection, in which the details can be clearly seen as overlapping (notice the reduced statistics, which is higher in (b) and (c) as they combine x-ray counts coming from all projections). (b) and (c) represent reconstructed slices at $z$ positions corresponding to fibres and discs, respectively. Details are clearly isolated while a strong phase contrast signal is preserved at the edges. This can be better appreciated in the profiles shown in panels (d), (e) and (f), which were extracted from images (a), (b) and (c) respectively at the positions indicated by the black horizontal lines.

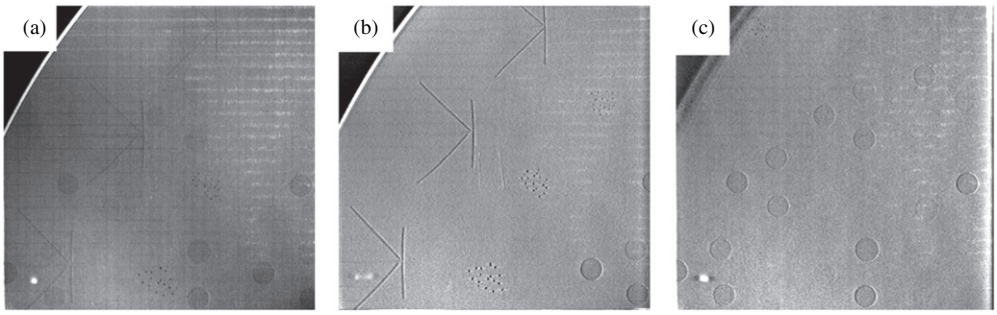


**Figure 6.** Full area of the 'double TORMAM' phantom that was imaged. (a) Single projection, (b) and (c) reconstructed slices. The horizontal lines are 'line interruptions' introduced in the masks to increase stability and adhesion to the substrate—in a commercial device these would have sub-pixel dimensions and therefore be eliminated through flat-fielding.

## Conclusions

We have conducted a preliminary phantom study on the possible implementation of the edge-illumination x-ray phase contrast imaging method in the tomosynthesis geometry. The goal was to use simple masks and a commercially available x-ray source and detector to perform a scan with exposure times and dose values not too distant from clinical requirements. The target was met in terms of delivered dose; however, it was only partially met in terms of exposure

time. Nevertheless, strategies can be implemented (reduction of the overall system length, use of different anode material/design, etc), which could make the required $\sim 10\times$ reduction in exposure time possible.

In addition to this, we show that significant phase-induced edge enhancement is preserved in the reconstructed slices, and we discuss strategies to design a clinical system in which the source rotates and the patient is kept stationary. Finally, we have fully modelled the system using two different simulation codes, and demonstrated excellent agreement with the experimental results. These models will support the developments of the next stages (more complex phantoms, increased angular range/number of projections, etc) of what is admittedly a preliminary, yet encouraging, proof-of-concept investigation.

## Acknowledgments

This work is funded by EPSRC (grants EP/G004250/1 and EP/I021884/1). KI and part of the used equipment was funded by the Wellcome Trust (grant 085856/Z/08/Z). MBS was funded by an EPSRC-GB doctoral training allowance and by Dexela (now a Perkin Elmer company). McXtrace software can be found at http://www.mcxtrace.org. The reconstruction software was provided by Dexela.

## References

Bravin A, Coan P and Suortti P 2013 X-ray phase contrast imaging: from pre-clinical applications towards clinics *Phys. Med. Biol.* **58** R1–35

Castelli E *et al* 2011 Mammography with synchrotron radiation: first clinical experience with phase-detection technique *Radiology* **259** 684–94

Chapman D *et al* 1997 Diffraction enhanced x-ray imaging *Phys. Med. Biol.* **42** 2015–25

Davis T J, Gao D, Gureyev T E, Stevenson A W and Wilkins S W 1995 Phase-contrast imaging of weakly absorbing materials using hard x-rays *Nature* **373** 595–8

Diemoz P C *et al* 2013 X-ray phase-contrast imaging with nanoradian angular resolution *Phys. Rev. Lett.* **110** 138105

Dobbins J T and Godfrey D J 2003 Digital x-ray tomosynthesis: current state of the art and clinical potential *Phys. Med. Biol.* **48** R65–106

Erdogan H and Fessler J A 1999 Monotonic algorithms for transmission tomography *IEEE Trans. Med. Imaging* **18** 801–14

Fessler J A and Erdogan H 1999 A paraboloidal surrogates algorithm for convergent penalized-likelihood emission image reconstruction *Proc. 1998 IEEE Nuclear Science Symp. and Medical Imaging Conf.* (Toronto: Canada) vol 2 pp 1132–5

Gennaro G, Baldelli P, Taibi A, Di Maggio C and Gambaccini M 2004 Patient dose in full-field digital mammography: an Italian survey *Eur. Radiol.* **14** 645–52

Ignatyev K, Munro P R T, Chana D, Speller R D and Olivo A 2011a Coded apertures allow high-energy x-ray phase contrast imaging with laboratory sources *J. Appl. Phys.* **110** 014906

Ignatyev K, Munro P R T, Speller R D and Olivo A 2011b Effects of signal diffusion on x-ray phase contrast images *Rev. Sci. Instrum.* **82** 073702

Ignatyev K, Olivo A, Munro P and Speller R 2013 X-ray imaging *International Patent* WO/2013/011316

Ingal V N and Beliaevskaya E A 1995 X-ray plane-wave topography observation of the phase contrast from a non-crystalline object *J. Phys. D: Appl. Phys.* **28** 2314–7

Knudsen E B *et al* 2011 McXtrace: a modern ray-tracing package for x-ray instrumentation *Proc. SPIE* **8141** 81410G

Köhler T, Brendel B and Roessl E 2011 Iterative reconstruction for differential phase contrast imaging using spherically symmetric basis functions *Med. Phys.* **38** 4542–5

Lewis R A 2004 Medical phase contrast x-ray imaging: current status and future prospects *Phys. Med. Biol.* **49** 3573–83

Marenzana M *et al* 2012 Visualization of small lesions in rat cartilage by means of laboratory-based x-ray phase contrast imaging *Phys. Med. Biol.* **57** 8173–84

Munro P R T, Hagen C K, Szafraniec M B and Olivo A 2013 A simplified approach to quantitative coded aperture x-ray phase imaging *Opt. Exp.* **21** 11187–201

Munro P R T, Ignatyev K, Speller R D and Olivo A 2010 The relationship between wave and geometrical optics models of coded aperture type x-ray phase contrast imaging systems *Opt. Exp.* **18** 4103–17

Munro P R T, Ignatyev K, Speller R D and Olivo A 2012a Phase and absorption retrieval using incoherent x-ray sources *Proc. Natl Acad. Sci. USA* **109** 13922–7

Munro P R T *et al* 2012b 'Edge illumination' in x-ray phase contrast imaging *AIP Conf. Proc.* **1466** 118–23

Niklason L T *et al* 1997 Digital tomosynthesis in breast imaging *Radiology* **205** 399–406 (PMID: 9356620)

Olivo A, Ignatyev K, Munro P R T and Speller R D 2011a Noninterferometric phase-contrast images obtained with incoherent x-ray sources *Appl. Opt.* **50** 1765–9

Olivo A, Ignatyev K, Munro P R T and Speller R D 2011b A coded-aperture based method allowing non-interferometric phase contrast imaging with incoherent x-ray sources *Nucl. Instrum. Methods* A **648** S28–31

Olivo A and Speller R 2007a A coded-aperture technique allowing x-ray phase contrast imaging with conventional sources *Appl. Phys. Lett.* **91** 074106

Olivo A and Speller R 2007b Modelling of a novel x-ray phase contrast imaging technique based on coded apertures *Phys. Med. Biol.* **52** 6555–73

Olivo A and Speller R 2008 Image formation principles in coded-aperture based x-ray phase contrast imaging *Phys. Med. Biol.* **53** 6461–74

Olivo A *et al* 2001 An innovative digital imaging set up allowing a low-dose approach to phase contrast applications in the medical field *Med. Phys.* **28** 1610–9

Park J M, Franken E A, Garg M, Fajardo L L and Niklason L T 2007 Breast tomosynthesis: present considerations and future applications *Radiographics* **27** S231–40

Pfeiffer F, Weitkamp T, Bunk O and David C 2006 Phase retrieval and differential phase-contrast imaging with low-brilliance x-ray sources *Nature Phys.* **2** 258–61

Snigirev A, Snigireva I, Kohn V, Kuznetsov S and Schelokov I 1995 On the possibilities of x-ray phase contrast microimaging by coherent high-energy synchrotron radiation *Rev. Sci. Instrum.* **66** 5486–92

Sottivirat S and Fessler J A 2000 Partitioned separable paraboloidal surrogate coordinate ascent algorithm for image restoration *Proc. Intl. Conf. on Image Processing (ICIP 2000)* (Vancouver: Canada) vol 1 pp 109–12

Wilkins S W, Gureyev T E, Gao D, Pogany A and Stevenson A W 1996 Phase-contrast imaging using polychromatic hard x-rays *Nature* **384** 335–8

Zambelli J, Bevins N, Zhihua Q and Chen G 2010 Radiation dose efficiency comparison between differential phase contrast CT and conventional absorption CT *Med. Phys.* **37** 2473–9